Humidity and Solvent Effects in Spin-Coated Polythiophene–Polystyrene Blends

J. Jaczewska,[1] A. Budkowski,[1] A. Bernasik,[2] I. Raptis,[3] J. Raczkowska,[1] D. Goustouridis,[3] J. Rysz,[1] M. Sanopoulou[4]

[1]*M. Smoluchowski Institute of Physics, Jagellonian University, Reymonta 4, 30-059 Kraków, Poland*
[2]*Faculty of Physics and Applied Computer Science, University of Science and Technology, Mickiewicza 39, 30-059 Kraków, Poland*
[3]*Institute of Microelectronics, National Centre for Scientific Research Demokritos, 15310 Aghia Paraskevi, Athens, Greece*
[4]*Institute of Physical Chemistry, National Centre for Scientific Research Demokritos, 15310 Aghia Paraskevi, Athens, Greece*

Received 11 March 2006; accepted 6 June 2006
DOI 10.1002/app.26012
Published online in Wiley InterScience (www.interscience.wiley.com).

ABSTRACT: Film blends of poly(3-butyltiophene-2,5-diyl) (PT) and polystyrene (PS; 1 : 1 w/w) were spin-coated onto silicon wafers from chloroform, tetrahydrofuran, and cyclohexanone at a controlled relative humidity between 4 and 86%. The film morphologies were determined with atomic and lateral force microscopy and mapping and depth profiling modes of dynamic secondary-ion mass spectroscopy. Independently, white light interferometry was used to examine the expansion and response time (τ) of pure polymer layers exposed to solvent vapors and moisture. The higher PS solubility, in comparison with the PT solubility, in chloroform and tetrahydrofuran resulted in PS/PT//Si bilayers, which were the final structures for coatings from chloroform [with much larger τ(PS)/τ(PT) ratios]. For tetrahydrofuran, these bilayers were destroyed, most likely by surface and interface instabilities, yielding hierarchic lateral structures. For cyclohexanone (with the largest τ values), a large-scale component of the lateral structures was absent, and this suggested the leveling of surface instabilities. The humidity changed the structural scales and thickness of the films cast from tetrahydrofuran (because it had the best solubility with water). The humidity effects of chloroform and cyclohexanone [reported earlier for polyaniline and poly(vinyl pyridine) blends] were practically absent. Moisture was not easily absorbed by PT and PS [in contrast to polyaniline and poly(vinyl pyridine)] and probably adsorbed merely at the surfaces of blend films rich in tetrahydrofuran. © 2007 Wiley Periodicals, Inc. J Appl Polym Sci 105: 67–79, 2007

Key words: blending; conjugated polymers; phase separation; spin coating; thin films

INTRODUCTION

Thin polymer films are commonly prepared by spin coating: A polymer solution is deposited onto the substrate, which is then rotated to produce homogeneous submicrometer films. Their thickness is controlled by the coating speed and polymer concentration in the solution.[1] When two (or more) polymers dissolve in the same solvent, they can be deposited simultaneously during the same spin-casting process. Such a blending strategy results in mixtures with novel structural and physical properties distinct from those of the pure polymers. Phase separation, initiated by solvent evaporation during spin casting, involves complex, non-quasi-static processes[2–8] different from those in the bulk and films exposed to elevated temperatures.[9–12] These not completely resolved processes result in various morphologies of spin-coated blend films that are dependent on the exact casting conditions. Three general types of ordered phase domain structures have been reported. Self-stratified films with vertical lamellar structures have been observed for spin-cast binary mixtures [insulating–insulating (I–I),[13–15] insulating–conjugated (I–C),[16] conjugated–conjugated (C–C),[17–20] and conjugated–nanoparticle (C–N)[21,22]] of insulating and/or conjugated polymers and molecules or nanoparticles. Alternatively, lateral morphologies with in-plane structures have been obtained for the same or similar systems (I–I,[2–6,8,14,15,23–28] I–C,[29–31] C–C,[7,20,32,33] and C–N[34,35]). Finally, under specific circumstances, laterally arranged phase domains have been observed to

This article is dedicated to the memory of Professor Marian Kryszewski.

Correspondence to: A. Budkowski (ufbudkow@cyf-kr.edu.pl).

Contract grant sponsor: Reserve of the Faculty of Physics, Astronomy, and Applied Computer Science of Jagellonian University.
Contract grant sponsor: Polish Committee for Scientific Research; contract grant number: 3 T08C 032 27.
Contract grant sponsor: Greek–Polish Bilateral Cooperation Agreement.

replicate the substrate pattern predefined by soft lithography (see the reports for I–I,[14,36–41] C–C,[42] and I–N mixtures[43]).

From an application viewpoint, the spin coating of polymer blends is a one-step process to deposit and align simultaneously domains rich in different polymers, which might form various functional elements of potential hi-tech devices. Lamellar structures that form during spin casting have been proposed to produce field-effect transistors,[21] polymer-covered liquid-crystal displays,[44] and efficient[12,45] light-emitting diodes (LEDs)[18] and photodiodes.[17] In turn, in-plane film morphologies have been shown to result in high-performance antireflection coatings[28] and polymer LEDs with voltage-controlled color.[32] Also, blends of conjugated polythiophene and insulating polymers, similar to those examined in this study, have been reported to yield lateral structures applicable to the production of anisotropic conductors, submicrometer-size LEDs, and LEDs with white-light emissions or improved voltage-controlled color.[29,30,46] Finally, the substrate-pattern-controlled domain arrangement of spin-cast blends has been used to create photonic structures, increasing the efficiency of polymer LEDs.[42]

It is obvious that understanding and controlling the blend film morphology can significantly contribute to the optimization of various hi-tech devices. However, although the literature indicates impressive technological developments obtained for spin-cast polymer blends, much less has been done to examine systematically the effects of the exact casting conditions, including the impact of humidity. Humidity effects on film morphology have been reported for pure polymers cast from tetrahydrofuran (THF),[47,48] polystyrene–poly(methyl methacrylate)–poly(vinyl pyridine) (PS–PMMA–PVP) ternary mixtures cast from cyclohexanone,[4] and polyaniline–polystyrene (PANI–PS) binary blends cast from chloroform.[31] Only extreme cases of low and high humidity have been examined for polymer mixtures:[4,31] A more humid atmosphere introduces the separation of poly(vinyl pyridine) (PVP) domains from polystyrene (PS) matrices by poly(methyl methacrylate) (PMMA)-rich rings in the lateral structures of PS–PMMA–PVP.[4] In turn, high humidity destroys the multilayer structure of PANI–PS, separates polyaniline (PANI) from its dopant, and results in lateral structures.[31]

In this work, we present systematic studies of the humidity (and solvent) effects on the film morphology of poly(3-butyltiophene-2,5-diyl)–polystyrene (PT–PS) blends spin-cast from common solvents: chloroform, THF, and cyclohexanone. Film structures were determined with atomic force microscopy (AFM) and lateral force microscopy (LFM)[37,39,41,49] as well as depth profiling and mapping modes of dynamic secondary-ion mass spectroscopy (dSIMS).[16,31,50] The important parameters for film-structure formation in spin-cast polymer blends are the relative solubility and relative desorption/absorption of a common solvent by different polymers.[24,27,51] To relate the determined PT–PS blend morphologies, which are different for the various solvents used, to the relevant film-formation mechanisms[2–8] we have examined with white light interferometry[52,53] the film expansion and response time (τ) of pure polymer layers exposed to solvent vapors (and to humidity). The interferometry data are introduced before the morphologies of the spin-cast blends are presented and discussed. The humidity drastically modifies the film structure of PT–PS blends cast from THF and has hardly any effect on PT–PS mixtures coated from chloroform and cyclohexanone (in contrast to reports on PANI–PS[31] and PS–PMMA–PVP[4]). This is explained by the relative best solubility of THF and water [and much smaller swelling of poly(3-butyltiophene-2,5-diyl) (PT), PS, and PMMA in a humid atmosphere in comparison with PANI and PVP].

EXPERIMENTAL

Materials

The polymers used in this work were regiorandom PT and PS [weight-average molecular weight (M_w) = 65,000, weight-average molecular weight/number-average molecular weight (M_w/M_n; i.e., polydispersity index) = 1.02]. The swelling of films exposed to moisture was evaluated also for PANI (M_w = 5000), PVP (M_w = 115,000, M_w/M_n = 1.03), and PMMA (M_w = 65,000, M_w/M_n = 1.05). PT and PANI were purchased from Aldrich, whereas other polymers were purchased from Polymer Standard Service (Mainz, Germany). The polymers were dissolved in analytical-grade common solvents (chloroform, THF, and cyclohexanone) to form solutions of pure polymers (with a concentration of $\sim$ 30 mg/mL) and symmetric (1 : 1 w/w) polymer blends (with a constant concentration of 20 mg/mL). Only PANI, additionally doped with camphorsulfonic acid, formed a chloroform solution with a concentration of 4 mg/mL.[31]

Film-swelling evaluation

Pure polymer films were spin-cast (coating speed = 3000 rpm) onto thermally oxidized silicon wafers with a 1050-nm-thick silicon dioxide layer and post-baked at 120°C for 15 min. Such Si substrates with well-controlled, micrometer-thick SiO2 layers were required to obtain interference fringes in the spectrum of white light (with an AvaLight HAL tungsten halogen visible/near-infrared source) reflected from the substrates with deposited polymer layers with an average thickness (d_0) of 190–250 nm. The reflected light was compared with the light source using the

USB SD2000 spectrophotometer (Ocean Optics, Dunedin, FL) (with a 0.4-nm resolution). The normalized interference spectrum, recorded at intervals of 1.2 s, was analyzed to monitor in real time the optical thickness of the polymer films and the evolution of the normalized film thickness (d/d_0) with time (a constant refractive index was assumed). The temporal thickness evolution [$d/d_0(t)$] was determined for the polymer films exposed (at $t = 0$ min) to nitrogen flux with a predetermined molar fraction of the solution vapor or humidity (for details, see refs. 52 and 53). The temperature of the gas environment inside the sample chamber was 25°C. The temperature of the polymer film was 30°C.

Film-morphology examination

PT–PS blend films were spin-coated at room temperature (constant coating speed = 3500 rpm for 30 s) from different solvents (polymer concentration = 20 mg/mL) onto silicon wafers with a native SiO_x layer with a KW-4A coater from Chemat Technology (Northridge, CA). Before the spin casting, the relative humidity (RH; 4–61%) was adjusted by a nitrogen flux of fixed humidity through the coating bowl. A very humid atmosphere (RH > 61%) was obtained and controlled by a hot-water beaker placed in the bowl. The bowl had a small opening to drop the solution onto the substrate with a Pasteur pipette. The RH was monitored by a humidity sensor (located close to a spinning substrate) and was constant during the spin-casting process. Additional (test) blend films were prepared from denser (polymer concentration = 35 mg/mL) cyclohexanone solutions or at a reduced coating speed (<3500 rpm).

Topographic and friction surface images of the cast thin films were collected in air at room temperature in AFM and LFM force modes of an Academia system microscope (Nanonics Imaging, Ltd., Jerusalem, Israel; scan range up to 70 μm × 70 μm) working in the contact mode. Test measurements were made with a MultiView 1000 microscope (Nanonics Imaging). LFM resolved domains rich in different polymers.[49] The average film thickness was determined from AFM images taken after partial film removal.[49] The characteristic length scale of the lateral structure was determined from two-dimensional fast Fourier transforms of AFM images when statistically significant data were available.[27,49]

Vertical and horizontal aspects of the phase domain structure in the blend films were provided by mapping[50] and depth profiling (depth resolution ~ 10 nm)[16,31] modes of dSIMS. The dSIMS data were obtained with a VSW apparatus equipped with a high-resolution ion gun (liquid metal; Fei Co., Hillsboro, OR) and a Balzers quadrupole mass spectrometer. A primary Ga^+-ion beam (5–25 keV, 0.2–4 nA) was used to sputter the sample and to induce secondary ions, which yielded mass-resolved information for the maps and the depth profiles. The maps of PT (S^- ions, $m/z = 32$) or all the polymers (C_2^-, $m/z = 24$) as well as the profiles of Si (Si^-, $m/z = 28$) and all the polymers (C_2^-) were provided by individual signals. To obtain a measure related to the average fractional concentration of PT in a polymer film as a function of depth, the original S^- signal ($m/z = 32$) was normalized by the $m/z = 24$ yield. A few composition maps of PT or all polymers were collected for successive sections in the analyzed samples with increasing distance z' from the surface.

RESULTS

Swelling of the pure polymers exposed to humidity and solvent vapors

Film expansion measurements were performed for volatile compounds with an actual partial pressure (p) much lower than the saturated vapor pressure (p_V). This was to avoid lateral (and not vertical) swelling as well as uncontrolled droplet condensation. Earlier experiments using this technique[52–56] for polymer films have shown that the film expansion is constant for films thicker than ~ 100 nm (as used here, except for PANI), whereas finite size effects can increase this value by 50–90% for thinner films (with $d_0 \sim 50$ nm,[52] as obtained for PANI) positioned on silicon (di)oxide substrates.

Because the swelling of the polymer films exposed to a humid atmosphere was relatively low, we have not determined response time τ for the introduced humidity. The results, illustrated by Figure 1(a), show three consecutive time periods with ambient RH values of 0, 11, and 22%. For PANI, only two periods were applied with RH values of 0 and 22%. These data, summarized in Table I, indicate negligible moisture absorption for nonpolar PS with a relative expansion of $(d - d_0)/d_0 < 0.1\%$. The water uptake is also very low for PT and PMMA [with $(d - d_0)/d_0 \sim 0.3\%$]. In contrast, water absorption is a few times higher for both PVP and PANI with $(d - d_0)/d_0$ reaching a percentage level (even for PANI after renormalization to thick films). We will come back to these results in the Discussion section.

$d/d_0(t)$ of PT and PS films exposed (at $t = 0$ min) to solvent vapors of chloroform ($p/p_V = 0.08$), THF ($p/p_V = 0.09$), and cyclohexanone ($p/p_V = 0.10$) is presented in Figures 1(b–d), respectively. We notice at once that the film swelling (see also Table I) and hence absorption of chloroform and THF are higher for PS than PT. This could be translated into solvent quality[57] or solubility[58] relations. The swelling results show that chloroform and THF are better solvents for PS than PT. The same should be true also for cyclo-

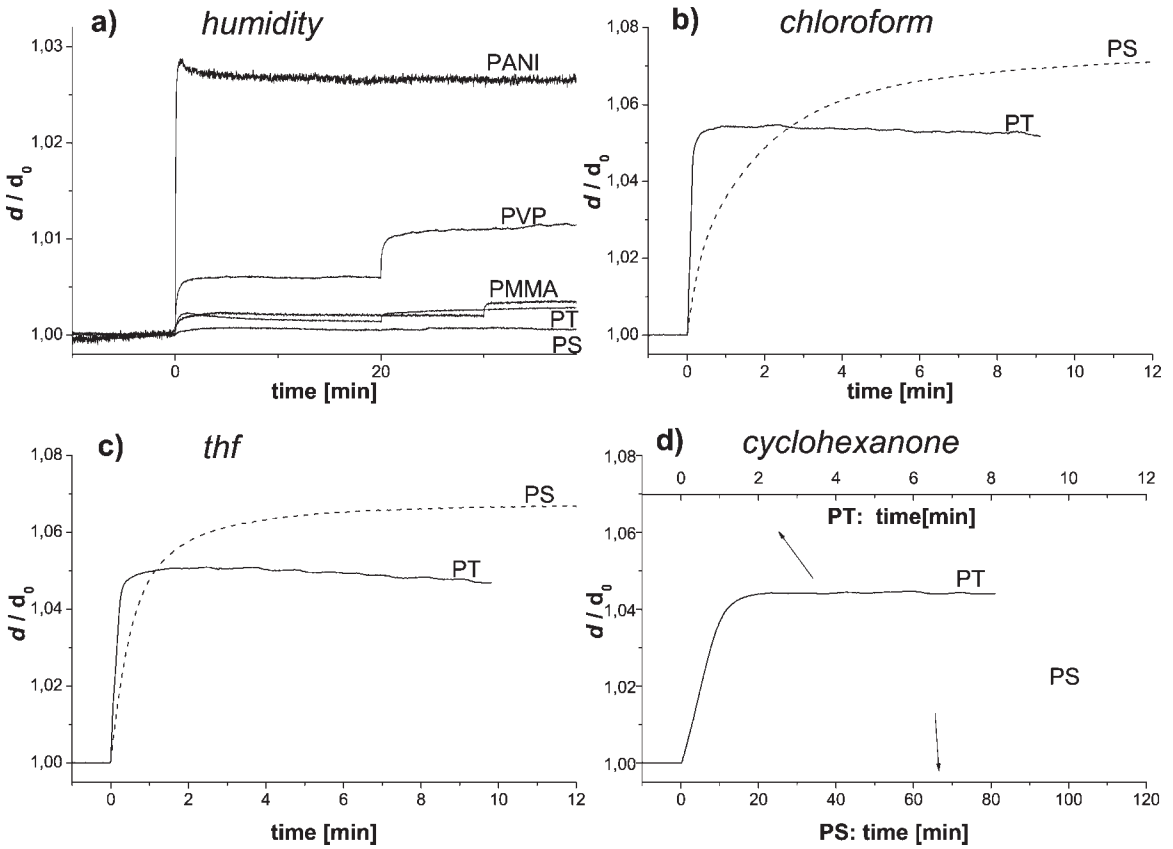

Figure 1 $d/d_0(t)$ determined for polymer films exposed to (a) humidity, (b) chloroform, (c) THF and (d) cyclohexanone. In part a, three consecutive periods (two for PANI) with ambient RH values of 0, 11, and 22% (0 and 22% for PANI) were applied to evaluate the water uptake by PS, PT, PMMA, PVP, and PANI. In parts b–d, PT and PS were exposed (at $t = 0$ min) to solvent vapors with p equal to 0.08 p_V, 0.09 p_V, and 0.10 p_V for chloroform, THF, and cyclohexanone, respectively.

hexanone because the solubility parameters increase in the following order: PS < chloroform < THF < cyclohexanone.[58] This conclusion cannot be deduced directly from swelling experiments [Fig. 1(d)] as the extremely sluggish reaction of PS exposed to cyclohexanone prevents a reliable evaluation of the equilibrium d/d_0 value.

Thickness–time curves, presented in Figure 1(b–d), show that τ for the polymer films to the introduced solvent vapors is always much longer for PS than PT. The exact values of τ, defined as the period between 10 and 90% of the expansion change, are presented in Table I. For chloroform and THF, which are more volatile solvents, we have τ(PS)/τ(PT) values of ~ 36 and ~ 9, respectively. In turn, for cyclohexanone, with p_V some 27–33 times lower, the τ values are much larger for both PT and PS, in line with the higher molar volume of this solvent in comparison with THF and chloroform. In addition, we observe here again τ(PS) > τ(PT). Earlier studies[53] on the swelling kinetics of

TABLE I
$(d - d_0)/d_0$ and τ Values of the Pure Polymer Films ($190 < d_0 < 250$ nm) Exposed to Volatile Compounds

		PT	PS	PMMA	PVP	PANI
Water (11% RH)	$(d - d_0)/d_0$ (%)	0.2	<0.1	0.2	0.6	
Water (22% RH)	$(d - d_0)/d_0$ (%)	0.3	<0.1	0.3	1.1	2.8[b]
Chloroform (8% *Pv*)	$(d - d_0)/d_0$ (%)	5.4	7.3			
	τ (min)[a]	0.15	5.4			
THF (9% *Pv*)	$(d - d_0)/d_0$ (%)	5.1	6.7			
	τ (min)[a]	0.3	2.7			
Cyclohexanone (10% *Pv*)	$(d - d_0)/d_0$ (%)	4.4	—			
	τ (min)[a]	1.0	>85			

[a] τ is defined as the period between 10 and 90% of the expansion change. The RH and p/pV values were rescaled to a polymer sample temperature of 30°C.[54]
[b] For $d_0 = 46$ nm.

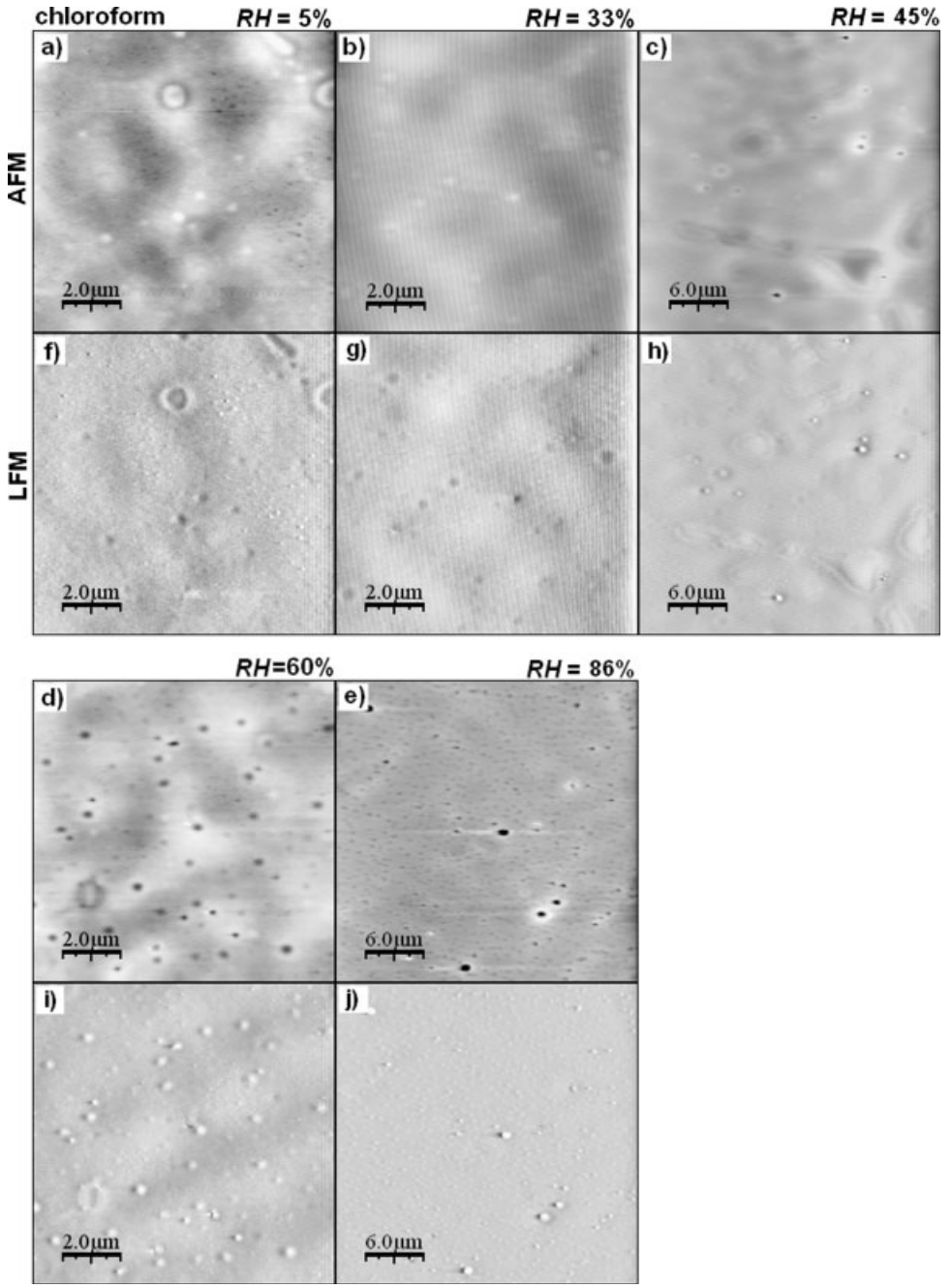

Figure 2 (a–e) AFM and (f–j) LFM surface images collected simultaneously for PT–PS blends spin-cast from chloroform at RH values of (a,f) 5, (b,g) 33, (c,h) 45, (d,i) 60, and (e,j) 86%. The gray level depicts the height (AFM) or LFM signal scale (white corresponds to high values). To maximize the AFM contrast, a height range of 20 nm was applied.

polymer films exposed to repeated periods of zero and nonzero concentrations of volatile compounds have shown that the absorption (film expansion) and desorption (film contraction) τ values are comparable. For this reason, we believe that the τ relations between expanding PT and PS films (determined here for different absorbed solvents) will hold also for desorbing polymers, that is, for the case relevant for film-structure formation during spin casting (see the Discussion section).

Humidity effects on the blend film morphology

We introduce now the morphologies of the PT–PS blend films coated from three different solvents and examine the effects of the humidity on the resulting film structures. The solvents have comparable solubility parameters (19.0, 19.4, and 19.6 $MPa^{1/2}$ for chloroform, THF, and cyclohexanone, respectively[58]) and were reported earlier to show moisture-dependent morphologies for spin-cast polymer films.[4,31,47,48] The

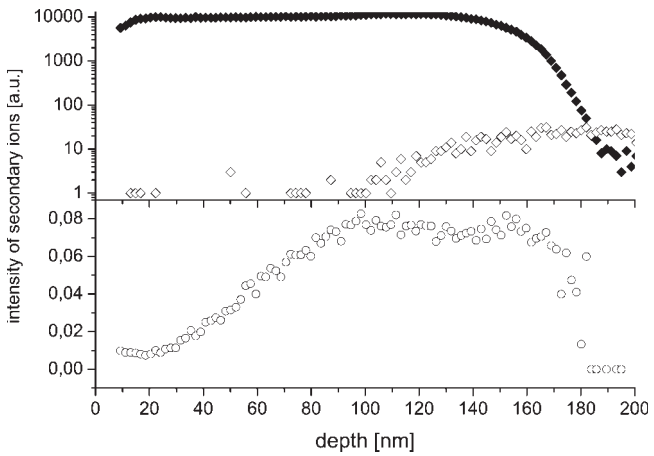

Figure 3 Depth dSIMS profiles recorded for PT–PS blends spin-cast (at RH = 60%) from chloroform and corresponding to (◆) the total polymer composition ($m/z = 24$) and (◇) the average Si concentration ($m/z = 28$) as well as (○) the fraction of PT in the polymer film ($m/z = 32$, normalized by $m/z = 24$).

results for the PT–PS film morphology are discussed together in the Discussion section.

Coatings from chloroform

Representative surface morphologies determined with AFM for PT–PS films cast from chloroform under dry, intermediate, and humid conditions (5, 33–45, and 60–86% RH, respectively) are shown in Figure 2(a–e). The corresponding LFM images are presented in Figure 2(f–j). The surface was only weakly fluctuating (amplitude < 5 nm). The humidity had no effect on the surface morphology, except for very weak secondary features [submicrometer, shallow holes; cf. Fig. 2(d,e) and 2(a–c)]. In addition to predominantly flat surface regions, optical microscopy revealed large-scale surface corrugations (due to hydrodynamic instabilities) commonly reported for rapidly evaporating solvents.[59,60]

The LFM images [Fig. 2(f–j)] show only very weak modifications of the lateral force signal and suggest that the surface of PT–PS blends, cast under different humidity conditions, was covered by the same continuous polymer domain. This was confirmed by the profiling dSIMS mode. The dSIMS results are exemplified by the data obtained at RH = 60% (Fig. 3). The depth profile of C_2^- secondary ions, corresponding to all polymers, is relatively constant and decays only at the onset of the Si− substrate signal, indicating the absence of any lateral polymer film structures.[5,6] In turn, the depth profile of the fractional PT concentration in the polymer film (provided by the S^- yield normalized by the C_2^- signal) reveals clearly the PS/PT//Si bilayer morphology. An apparently large interfacial width of 25.0 (1.6) nm suggests an undulating PS/PT interface. A strongly undulating PS/PT interface (as well as large-scale surface corrugations) is reflected by the relatively extended sputtering period corresponding to the decay of C_2^- at the onset of the Si^- signal.

The dSIMS profiles obtained under lower humidity are similar to those of Figure 3. Even the apparent interfacial width [24.3 (2.0) nm at RH = 5%] is (within the error bars) unchanged. Also, film thickness d_0 = 130 (20) nm does not react to humidity variations [Fig. 4(a)]. We conclude that moisture has no effect here on the film morphology.

Coatings from THF

Figure 5 depicts surface morphologies recorded simultaneously with AFM [Fig. 5(a–e)] and LFM [Fig. 5(f–j)] for PT–PS blend films spin-coated from THF at low and intermediate [Fig. 5(a–c,f–h)], high [Fig. 5(d,i)], and very high [Fig. 5(e,j)] humidities. Topographic patterns recorded with AFM correspond to the morphologies resolved by LFM, which might reflect lateral domains rich in PT and PS.

To identify the LFM contrast and to check the vertical extent of the lateral structures, the imaging dSIMS mode was applied. Imaging dSIMS results are presented in Figure 6 by the data set determined for the PT–PS film cast from THF at RH = 40%. The four composition maps of PT [yielded by S^- ions; Fig. 6(a,c)] and of all the polymers [given by the C_2^- signal; Fig. 6(b,d)] correspond to the subsequent sections of the blend film. The PT distribution maps,

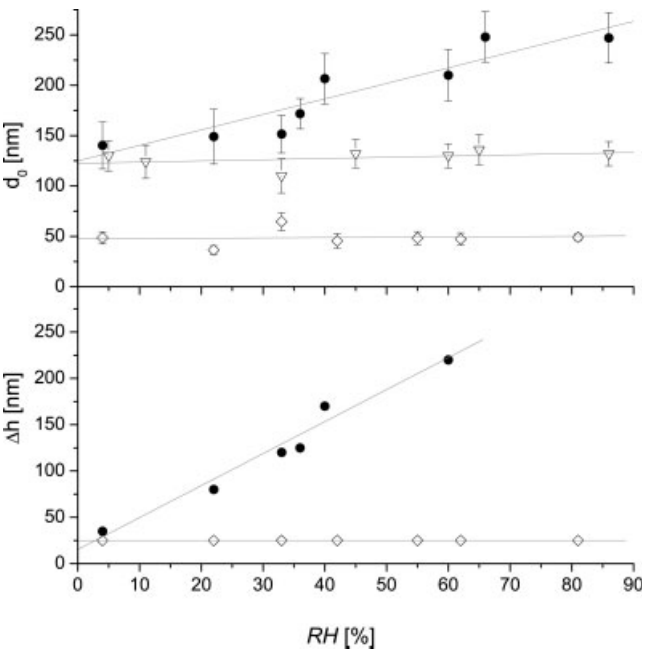

Figure 4 (a) d_0 and (b) Δh of topographic surface patterns as functions of RH for PT–PS blends spin-cast from (▽) chloroform, (●) THF, and (◇) cyclohexanone. The lines are guides for the eye.

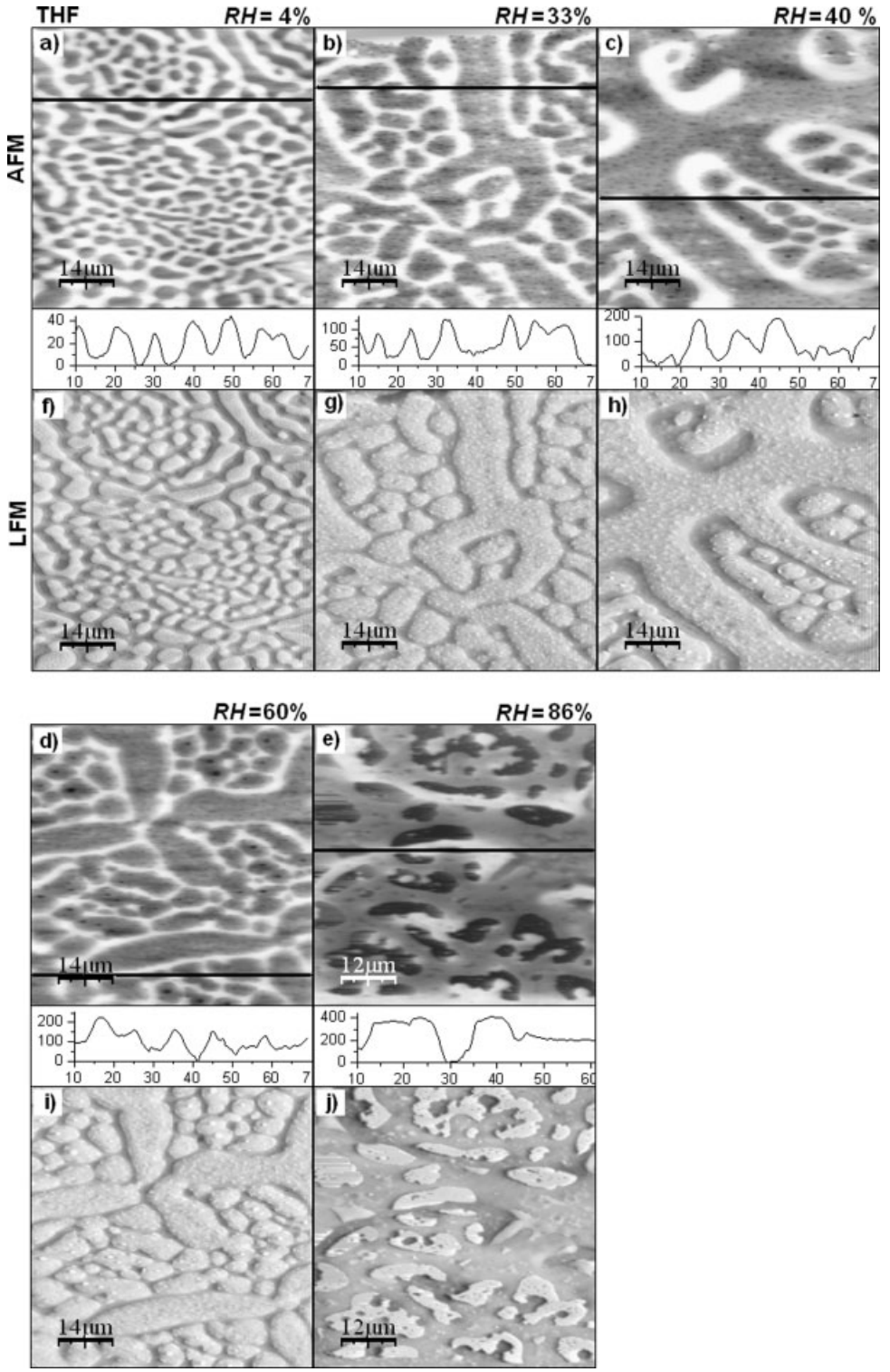

Figure 5 (a–e) AFM and (f–j) LFM surface images collected simultaneously for PT–PS blends spin-cast from THF at RH values of (a,f) 4, (b,g) 33, (c,h) 40, (d,i) 60, and (e,j) 86%. The sectional views correspond to the lines marked in the AFM images.

recorded for the sections adjacent to the surface [Fig. 6(a)] and substrate [Fig. 6(c)], have identical morphologies and show that the lateral phase structure extends from the surface throughout the film to the substrate. This morphology [Fig. 6(a,c)] matches that of AFM [Fig. 5(a–d)] and LFM [Fig. 5(f–i)] images: The surface regions with high PT concentrations are elevated and show lower LFM signals. In turn, PS-rich areas are depressed and exhibit higher LFM signals. The same is true for Figure 5(e,j), but

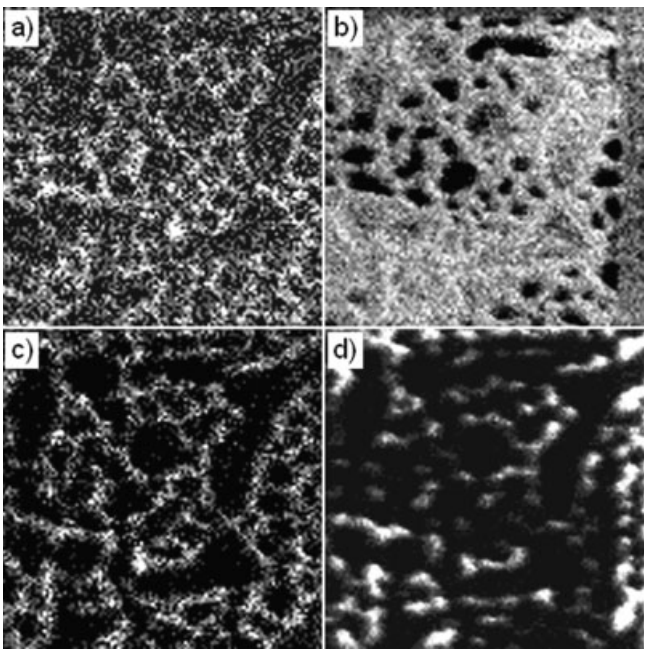

Figure 6 Composition maps (73 μm × 73 μm) of (a,c) PT (S− ions) and (b,d) all polymers (C_2^- ions) recorded for the subsequent sections of the PT–PS blend films cast from THF at RH = 40%. The lateral distributions correspond to average distances from the surface (z') of (a) ~ 26, (b) ~ 77, (c) ~ 129, and (d) ~ 181 nm. The gray level depicts the concentration scale (white corresponds to high values). The heterogeneous regions of map b are due to faster sputtering of thinner PS-rich domains.

here the AFM images show in addition deep holes corresponding to the bare substrate (with a very high LFM signal).

The hierarchic lateral structures visible in the micrographs (Figs. 5 and 6), except for the very humid atmosphere with RH = 86%, reveal two characteristic length scales with magnitudes of micrometers (shorter) and tens of micrometers (longer scale). Both lateral length scales grow significantly with the humidity and decrease slightly at the onset of water condensation, which introduces film perforations[47,48] and destroys hierarchic blend structures [see Fig. 5(e,j)]. For smaller RH values, submicrometer, shallow holes appear (similar to those observed for chloroform). These secondary surface features are most likely related to the onset of condensation. The rise of the humidity involves substantial increases in two vertical parameters: d_0 [see Fig. 4(a)] and the vertical extent (Δh) of the topographic surface pattern [Fig. 4(b)].

Coatings from cyclohexanone

Typical surface morphologies determined with AFM and LFM for PT–PS films cast from cyclohexanone under different humidity conditions (RH = 4–81%) are shown in Figure 7. The topographic patterns visible in the AFM images correlate with the lateral domain structures resolved by LFM. A PT distribution map, yielded by the imaging dSIMS mode with S^- ions, is presented in Figure 8. We conclude that higher (islands) and lower (matrix) surface regions (with lower and higher LFM signals) correspond to PT- and PS-rich phase domains, respectively. This confirms the correlation between AFM, LFM, and dSIMS signals, which was noted earlier for blend coatings from THF. The lateral structures created during spin casting from cyclohexanone (Fig. 7) revealed only one characteristic (shorter) length scale of 2.1 (0.6) μm (average value).

The blends cast from cyclohexanone formed relatively thin films with $d_0 \sim 40$ nm, at least 3 times smaller than those with the other two solvents. Also, Δh of the topographic surface pattern (~ 25 nm) was smaller than the lowest Δh value obtained for THF. A higher total polymer concentration or a lower spinning speed resulted in thicker (test) blend films with the same morphology, as shown in Figure 7.

Neither d_0 nor Δh of the topographic patterns was modified by the increased RH [see Fig. 4(a,b)]. Also, the lateral length scale was hardly changed with RH [the lateral length of 2.3 (0.6) μm, determined at RH < 44%, is (within the error bars) not much different from the value of 2.0 (0.5) μm averaged for RH > 44%].

DISCUSSION

Film-structure evolution

Although the phase-separation processes[2–8] that take place during spin casting have not been completely resolved, the consecutive stages of film-structure formation have been recognized[3–8,24] to involve (1) self-stratification of a transient multilayer[6,8] often broken up by (2) surface (convective)[4,5,61,62] and/or (3) interface (capillary)[3,4,6,8] instability, followed (or replaced) by (4) lateral (quasi-two-dimensional) phase coarsening.[23,24,27] The final surface topography often reflects the lateral domain structure as a result of (5) different (for various polymer phases) vitrification rates and polymer swelling in the remaining solvent.[6,24,27,63] Such an overall structure evolution pattern (followed also by the PT–PS blends; Fig. 9) has been recently confirmed by a direct examination of the spin-casting process with light reflectivity and light scattering.[8]

The self-stratification process in spin-cast polymer blend films can be driven by different mechanisms,[16] such as polymer surface energy differences (wetting arguments[8,22]), specific polymer–substrate interactions,[14,31,39] and faster depletion of one blend component from a common solvent.[3,51,64] Neither the first nor second driving force can explain (at least alone) the film morphologies observed here, which are dif-

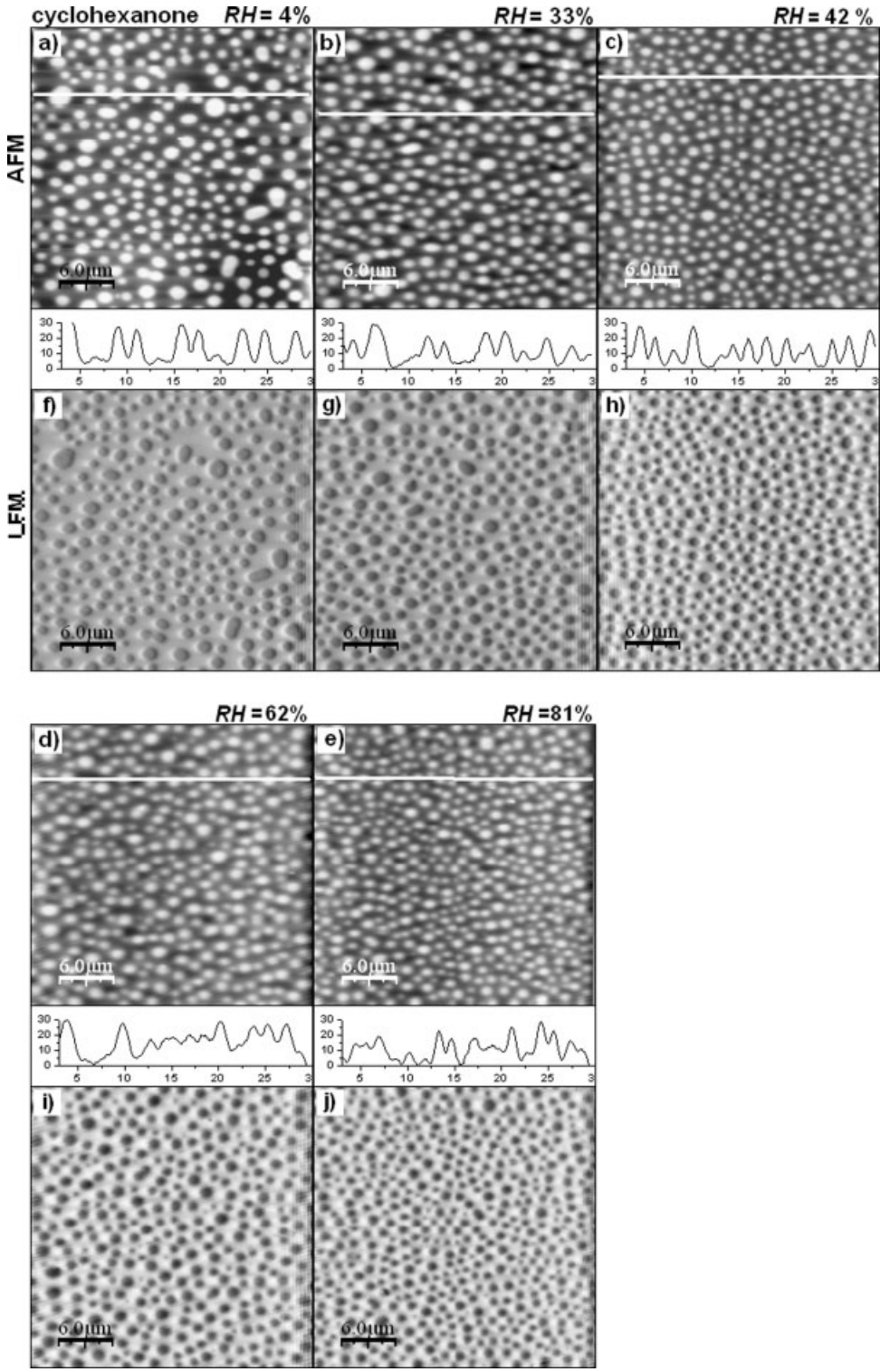

Figure 7 (a–e) AFM and (f–j) LFM surface images collected simultaneously for PT–PS blends spin-cast from cyclohexanone at RH values of (a,f) 4, (b,g) 33, (c,h) 42, (d,i) 62, and (e,j) 81%. The sectional views correspond to lines marked in the AFM images.

ferent for various solvents but similar for various substrates: PT–PS blend films cast from chloroform onto Au (not presented here) are identical to those coated onto Si (Figs. 2 and 3). Therefore, the last mechanism seems to be decisive here. According to the relevant scenario,[3,51] one polymer-rich phase is more quickly depleted from a homogeneous fluid film and deposited as a layer onto the substrate, whereas the second polymer-rich phase forms a second layer at the surface. The phase tendency to become depleted from

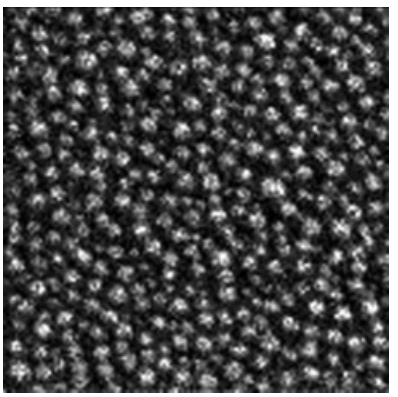

Figure 8 Composition map (73 μm × 73 μm) of PT (S^- ions) recorded for the PT–PS blend film cast (coating speed = 1300 rpm) from cyclohexanone at RH = 33%. The gray level depicts the concentration scale (white corresponds to high values).

the solvent-rich solution depends on the solvent flux to another phase (driven by lower solubility) and on the inherent solvent desorption time (faster desorption or a lower τ value of the pure polymer is preferred). The film-swelling results (see the previous paragraph) show a lower PT solubility in the common solvents used. In addition, the τ values were always lower for PT [Fig. 1(b–d) and Table I]. Both effects lead together to the formation of the substrate-adjacent PT-rich layer and hence to the creation of the overall bilayer structure PS/PT//Si [Fig. 9(b)]. Subsequent film-structure evolution depends not only on the ratio of the response (desorption) times from PT- and PS-rich phases but also on the overall evaporation rate from the whole blend film. The latter can be described as high for chloroform (with $Pv = 32.2$ kPa) and THF (26.7 kPa) but low for cyclohexanone (0.99 kPa).

The PS/PT//Si bilayer [Fig. 9(b)] was the final structure for the blends cast from rapidly evaporating chloroform; the large disparity in the solvent desorption rate from both polymer-rich phases was in addition suggested by the results obtained for the pure polymers [$\tau(PS)/\tau(PT) \sim 36$]. A much lower difference in the desorption rates [$\tau(PS)/\tau(PT) \sim 9$] for slightly less volatile THF made the bilayer prone to further structural evolution with effective surface and interface instabilities [Fig. 9(b–d)]. The bilayer structure could be broken up by both surface [Fig. 9(b–d)] and interface [Fig. 9(b–f)] instabilities, with two different characteristic wavelengths (tens of micrometers and micrometers, respectively[4]), often resulting in lateral hierarchic structures with two structural scales [Fig. 9(b–d)]. The surface instability is commonly related to a convective (hydrodynamic) mechanism[59,61,62] because of a temperature[61] or solvent concentration[62] gradient across the evaporating film. The related large-scale component of the hierarchic structure could be observed alone in pure polymer films spin-cast from rapidly evaporating solvents.[59,60] In contrast, such Marangoni patterns due to surface instability are absent[59,60] for the solvents with a low evaporation rate because the solvent-rich films now have time to level and heal the surface roughness[59] (alternatively, the solvent has time to diffuse and to remove the gradients driving the instability[8]). This is why the large-scale component of the hierarchic structure was absent here for the PT–PS blends spin-cast from cyclohexanone [Fig. 9(e,f)], for which τ (and

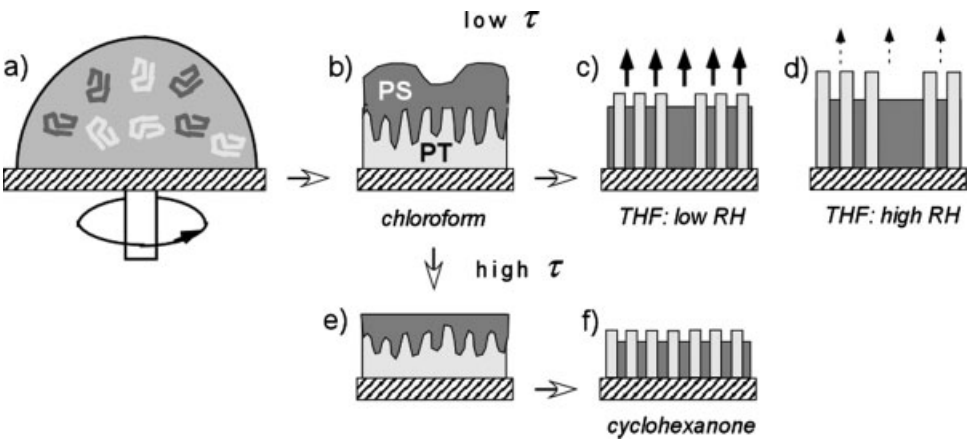

Figure 9 Schematic model describing film-structure formation during the spin casting of PT–PS blends from (a,b) chloroform, (a–c,d) THF, and (a,b,e,f) cyclohexanone. After (a) the spin-off stage, the film separates into (b) a bilayer with active surface (longer wavelength) and interfacial (shorter wavelength) instabilities leading to (c,d) hierarchic lateral structures. For the slow evaporation of the solvent, (e) the rough surface levels and (f) final structures show one (shorter) lateral length scale. The humidity, adsorbed by films cast from THF (with best solubility with water), reduces the solvent evaporation rate, leading to thicker films with larger lateral structural scales (cf. parts c and d). Faster desorption (shorter τ) for PT and better solubility for PS lead to PT depletion from the common solvent and to the creation of (b) a PT-rich substrate layer.

TABLE II
Characteristic Properties of the Solvents and Water

	Pv (kPa)[a]	δ (MPa$^{1/2}$)[b]	δ_d (MPa$^{1/2}$)[b]	δ_p (MPa$^{1/2}$)[b]	δ_h (MPa$^{1/2}$)[b]	$\Delta\delta_d$ (MPa$^{1/2}$)[c]	$\Delta\delta_{nd}$ (MPa$^{1/2}$)[d]
Chloroform	32.2	19.0	17.8	3.1	5.7	2.3	38.9
THF	26.7	19.4	16.8	5.7	8.0	1.3	35.9
Cyclohexanone	0.99	19.6	17.8	6.3	5.1	2.3	38.5
Water	4.24	47.9	15.5	16.0	42.4	—	—

[a] At 30°C.
[b] See ref. 58.
[c] $\Delta\delta_d^2 = [\delta_d - \delta_d(\text{water})]^2$.
[d] $\Delta\delta_{nd} = [\delta_p - \delta_p(\text{water})]^2 + [\delta_h - \delta_h(\text{water})]^2$.

hence also the evaporation) was at a least few times greater than that for the other solvents used. Because of slower cyclohexanone evaporation, the film-formation process on the spinning substrate was longer, and the resulting blend films were much thinner [Fig. 4(a)].

Finally, the surface topography of PT–PS blend films with a lateral morphology (for coatings from THF and cyclohexanone) reflected the lateral domain structure. The faster evaporating PT-rich domains vitrified earlier (as the τ data indicated) to form elevated surface regions, whereas the initially still swollen PS-rich phase collapsed below the level of PT-rich domains.

Humidity effects on the PT–PS blend film morphology

A film-morphology examination has shown that the humidity modifies dramatically the film structure of PT–PS blends coated from THF (Figs. 4 and 5) but has hardly any effect on PT–PS mixtures spin-cast from chloroform and cyclohexanone (Figs. 2, 4 and 7). In contrast, the earlier reports showed clearly the impact of the humidity on the morphology of polymer films spin-cast not only from THF (pure polymers[47,48]) but also from chloroform (PANI–PS mixtures[31]) and cyclohexanone (PS–PMMA–PVP blends[4]). To resolve this apparent discrepancy, we recall the swelling results for pure polymers exposed to moisture [Fig. 1(a) and Table I]. Humidity absorption was minimal for nonpolar PS, very low for PT and PMMA, and a few times higher for both PVP and PANI. It is evident that the previous results for PANI–PS and PS–PMMA–PVP polymer blends can be explained (as in the original publications[4,31]) by different (and controlled) water uptakes by various polymer-rich phases.

To explain the different results for the PT–PS blends spin-cast from various solvents, we have analyzed the solubility of these solvents with water (see Table II). The Hansen model,[58] with the three-component solubility parameter $\delta^2 = \delta_d^2 + \delta_p^2 + \delta_h^2$ (where δ_d is the dispersion component, δ_p is the polar component, and δ_h is the hydrogen component), was applied. The mutual solubility (between the ith and jth components) is high when the so-called Hansen distance (R_{ij}) is low:

$$R_{ij}^2 = A(\delta_{d,i} - \delta_{d,j})^2 + B[(\delta_{p,i} - \delta_{p,j})^2 + (\delta_{h,i} - \delta_{h,j})^2] = A\Delta\delta_d^2 + B\Delta\delta_{nd}^2 \quad (1)$$

Usually, the Hansen distance depends on two components, the dispersive component ($\Delta\delta_d$) and nondispersive component ($\Delta\delta_{nd}$), with *a priori* unknown constants A and B.[58] Therefore, we restrict our analysis to these two components of the Hansen distance between the water and the solvents used. The results of this examination, presented in Table II, show that minimal values of both $\Delta\delta_d$ (1.3 $<$ 2.3 MPa$^{1/2}$ for other solvents) and $\Delta\delta_{nd}$ (35.9 $<$ 38.5–38.9 MPa$^{1/2}$ for other solvents) can be concluded for THF.

The best THF solubility with water correlates well with the humidity effects observed for the PT–PS blends only when they were cast from this solvent. Because both polymers (PT and PS) practically do not absorb water, the humidity is most likely adsorbed at the surface of THF-rich blend films during the early stages [Fig. 9(b–d)] of spin casting (alternatively, the moisture concentration is increased in the air boundary layer above the THF-evaporating film[62]). Within such a model, the RH easily controls the solvent evaporation rate, higher RH values leading to thicker films with larger lateral structural scales [cf. Fig. 9(c,d)]. In an extremely humid atmosphere, blend films with the highest thickness are formed and are perforated additionally by water condensation.

CONCLUSIONS

The combination of a blend-morphology examination with a polymer-swelling evaluation, presented here (to the best of our knowledge) for the first time, provides us with insight into the film-structure formation of the same polymer blend spin-cast from different solvents. This might lead to improved morphological control of technologically important conjugated polymer blends, especially when the strategy of varying common solvents[17] is applied.

Visible (reported earlier[4,31]) and practically absent (this study for PT–PS mixtures) humidity effects in

blend films spin-cast from chloroform and cyclohexanone are explained by substantial and very small water uptakes, respectively, by the blend components (as indicated by swelling results). Hence, the large humidity impact on the PT–PS blends cast from THF must be explained by a novel mechanism involving preferential water adsorption at the surface of the blend film rich in THF. This mechanism is not active for larger Hansen distances between water and the common solvent used.

The results presented here indicate that humidity effects during the spin coating of polymer blends can be practically avoided for blend components with minimal water uptake and common solvents with large Hansen distances from water.

References

1. Lawrence, C. J. Phys Fluids 1998, 31, 2786.
2. Gutmann, J. S.; Müller-Buschbaum, P.; Stamm, M. Faraday Discuss 1999, 112, 258.
3. Ton-That, C.; Shard, A. G.; Teare, D. O. H.; Bradley, R. H. Polymer 2002, 43, 4973.
4. Sprenger, M.; Walheim, S.; Budkowski, A.; Steiner, U. Interface Sci 2003, 11, 225.
5. Budkowski, A.; Bernasik, A.; Cyganik, P.; Raczkowska, J.; Penc, B.; Bergues, B.; Kowalski, K.; Rysz, J.; Janik, J. Macromolecules 2003, 36, 4060.
6. Raczkowska, J.; Bernasik, A.; Budkowski, A.; Sajewicz, K.; Penc, B.; Lekki, J.; Lekka, M.; Rysz, J.; Kowalski, K.; Czuba, P. Macromolecules 2004, 37, 7308.
7. Jukes, P. C.; Heriot, S. Y.; Sharp, J. S.; Jones, R. A. L. Macromolecules 2005, 38, 2030.
8. Heriot, S. Y.; Jones, R. A. L. Nat Mater 2005, 4, 782.
9. Krausch, G. Mater Sci Eng R 1995, 14, 1.
10. Binder, K. Adv Polym Sci 1999, 138, 1.
11. Budkowski, A. Adv Polym Sci 1999, 148, 1.
12. Geoghegan, M.; Krausch, G. Prog Polym Sci 2003, 28, 261.
13. Geoghegan, M.; Jones, R. A. L.; Payne, R. S.; Sakellariou, P.; Clough, A. S.; Penfold, J. Polymer 1994, 35, 2019.
14. Böltau, M.; Walheim, S.; Mlynek, J.; Krausch, G.; Steiner, U. Nature 1998, 391, 877.
15. Ton-That, C.; Shard, A. G.; Daley, R.; Bradley, R. H. Macromolecules 2000, 33, 8455.
16. Bernasik, A.; Włodarczyk-Miskiewicz, J.; Łuzny, W.; Kowalski, K.; Raczkowska, J.; Rysz, J.; Budkowski, A. Synth Met 2004, 144, 253.
17. Arias, A. C.; Corcoran, N.; Banach, M.; MacKenzie, J. D.; Huck, W. T. S. Appl Phys Lett 2002, 80, 1695.
18. Corcoran, N.; Arias, A. C.; Kim, J. S.; MacKenzie, J. D.; Friend, R. H. Appl Phys Lett 2003, 82, 299.
19. Chappell, J.; Lidzey, D. G.; Jukes, P. C.; Higgins, A. M.; Thompson, R. L.; O'Connor, S.; Grizzim, I.; Fletcher, R.; O'Brien, J.; Geoghegan, M.; Jones, R. A. L. Nat Mater 2003, 2, 616.
20. Higgins, A. M.; Martin, S. J.; Thompson, R. L.; Chappell, J. C.; Voight, M.; Lidzey, D. G.; Jones, R. A. L.; Geoghegan, M. J Phys: Condens Matter 2005, 17, 1319.
21. Chua, L.-L.; Ho, P. K. H.; Sirringhaus, H.; Friend, R. H. Adv Mater 2004, 16, 1609.
22. Björström, C. M.; Bernasik, A.; Rysz, J.; Budkowski, A.; Nilsson, S.; Svensson, M.; Andersson, M. R.; Magnusson, K. O.; Moons, E. J Phys: Condens Matter 2005, 17, L529.
23. Dalnoki-Veress, K.; Dalnoki-Veress, K.; Forrest, J. A.; Stevens, J. R.; Dutcher, J. R. J Polym Sci Part B: Polym Phys 1996, 34, 3017.
24. Walheim, S.; Böltau, M.; Mlynek, J.; Krausch, G.; Steiner, U. Macromolecules 1997, 30, 4995.
25. Tanaka, K.; Takahara, A.; Kajiyama, T. Macromolecules 1996, 29, 3232.
26. Affrossman, S.; Henn, G.; O'Neill, S. A.; Pethrick, R. A.; Stamm, M. Macromolecules 1996, 29, 5010.
27. Raczkowska, J.; Rysz, J.; Budkowski, A.; Lekki, J.; Lekka, M.; Bernasik, A.; Kowalski, K.; Czuba, P. Macromolecules 2003, 36, 2419.
28. Walheim, S.; Schäffer, E.; Mlynek, J.; Steiner, U. Science 1999, 283, 520.
29. Grandström, M.; Berggren, M.; Pede, D.; Inganäs, O.; Andersson, M. R.; Hjertberg, T.; Wennerström, O.; Supramol Sci 1997, 4, 27.
30. Grandström, M.; Berggren, M.; Inganäs, O.; Andersson, M. R.; Hjertberg, T.; Wennerström, O. Synth Met 1997, 85, 1193.
31. Bernasik, A.; Haberko, J.; Wlodarczyk-Miskiewicz, J.; Raczkowska, J.; Luzny, W.; Budkowski, A.; Kowalski, K.; Rysz, J. Synth Met 2005, 155, 516.
32. Berggren, M.; Inganäs, O.; Gustafsson, G.; Rasmusson, J.; Andersson, M. R.; Hjertberg, T.; Wennerström, O. Nature 1994, 372, 444.
33. Morteani, A. C.; Dhoot, A. S.; Kim. J.-S.; Silva, C.; Greenham, N. C.; Murphy, C.; Moons, E.; Cina, S.; Burroughes, J. H.; Friend, R. H. Adv Mater 2003, 15, 1708.
34. Gebeyehu, D.; Brabec, C. J.; Padinger, F.; Fromherz, T.; Hummelen, J. C.; Badt, D.; Schindler, H.; Sariciftci, N. S. Synth Met 2001, 118, 1.
35. Björström, C. M.; Magnusson, K. O.; Moons, E. Synth Met 2005, 152, 109.
36. Sprenger, M.; Walheim, S.; Schäffer, C.; Steiner, U. Adv Mater 2003, 15, 703.
37. Cyganik, P.; Budkowski, A.; Steiner, U.; Rysz, J.; Bernasik, A.; Walheim, S.; Postawa, Z.; Raczkowska, J. Europhys Lett 2003, 62, 855.
38. Li, X.; Xing, R.; Zhang, Y.; Han, Y.; An, L. Polymer 2004, 45, 1637.
39. Raczkowska, J.; Cyganik, P.; Budkowski, A.; Bernasik, A.; Rysz, J.; Raptis, I.; Czuba, P.; Kowalski, K. Macromolecules 2005, 38, 8486.
40. Cui, L.; Zhang, Z.; Li, X.; Han, Y. Polym Bull 2005, 55, 131.
41. Raczkowska, J.; Bernasik, A.; Budkowski, A.; Cyganik, P.; Rysz, J.; Raptis, I.; Czuba, P. Surf Sci, 2006, 600, 1004.
42. Fichet, G.; Corcoran, N.; Ho, P. K. H.; Arias, A. C.; MacKenzie, J. D.; Huck, W. T. S., Friend, R. H. Adv Mater 2004, 16, 1908.
43. Minelli, C.; Geissbuehler, I.; Eckert, R.; Vogel, H.; Heinzelmann, H.; Liley, M. Colloid Polym Sci 2004, 282, 1274.
44. Pentermann, R.; Klink, S. I.; de Koning, Nosato; Nosato, G.; Broer, D. J. Nature 2002, 417, 55.
45. Moons, E. J Phys: Condens Matter 2002, 14, 12235.
46. Grandström, M.; Inganäs, O. Appl Phys Lett 1996, 68, 147.
47. Hecht, U.; Schilz, C. M.; Stratmann, M. Langmuir 1998, 14, 6743.
48. Park, M. S.; Kim, J. K. Langmuir 2004, 20, 5347.
49. Cyganik, P.; Budkowski, A.; Raczkowska, J.; Postawa, Z. Surf Sci 2002, 507, 700.
50. Bernasik, A.; Rysz, J.; Budkowski, A.; Kowalski, K.; Camra, J.; Jedlinski, J. Macromol Rapid Commun 2001, 22, 829.
51. Ton-That, C.; Shard, A. G.; Teare, D. O. H.; Bradley, R. H. Polymer 2001, 42, 1121.
52. Chatzandroulis, S.; Goustouridis, D.; Raptis; I.; Microelectron Eng 2005, 78, 118.
53. Goustouridis, D.; Manoli, K.; Chatzandroulis, S.; Sanopoulou, M.; Raptis, I. Sens Actuators 2005, 111, 549.
54. Elbs, H.; Krausch, G. Polymer 2004, 45, 7935.

55. Beck Tan, N. C.; Wu, W. L.; Wallace, W. E.; Davis, G. T. J Polym Sci Part B: Polym Phys 1997, 36, 155.
56. Vogt, B. D.; Soles, C. L.; Lee, H.-J.; Lin, E. K.; Wu, W. Polymer 2005, 46, 1635.
57. Teraoka, I. Polymer Solutions: An Introduction to Physical Properties; Wiley: New York, 2002.
58. Brandrup, I.; Immergut, E. H.; Grulke, E. A. Polymer Handbook, 4th ed.; Wiley: New York, 1999.
59. Strawhecker, K. E.; Kumar, S. K.; Douglas, J. F.; Karim, A. Macromolecules 2001, 34, 4669.
60. Müller-Buschbaum, P.; Gutmann, J. S.; Wolkenhauer, M.; Kraus, J.; Stamm, M.; Smilgies, D.; Petry, W. Macromolecules 2001, 34, 1369.
61. Mitov, Z.; Kumacheva, E. Phys Rev Lett 1998, 81, 3427.
62. de Gennes, P. G. Eur Phys J E 2001, 6, 421.
63. Elbs, H.; Funkunaga, K.; Stadler, R.; Sauer, G.; Magerle, R.; Krausch, G. Macromolecules 1999, 32, 1204.
64. Raczkowska, J.; Budkowski, A.; Rysz, J.; Czuba, P.; Lekka, M.; Bernasik, A. J Nanostruct Polym Nanocompos 2005, 1, 25.